STRUCTURAL CONTROL AND HEALTH MONITORING
Struct. Control Health Monit. 2015; **22**:1103–1118
Published online 10 February 2015 in Wiley Online Library (wileyonlinelibrary.com). DOI: 10.1002/stc.1735

Signal-based nonlinear modelling for damage assessment under variable temperature conditions by means of acousto-ultrasonics

M.-A. Torres-Arredondo[1,*,†], Julian Sierra-Pérez[2], D.-A. Tibaduiza[3], Malcolm McGugan[4], José Rodellar[5] and C.-P. Fritzen[6,7]

[1]*MAN Diesel & Turbo SE, Engineering 4 Stroke-Test and Validation-Test Bed Management-Measurement (EETTM), D-86224 Augsburg, Germany*
[2]*Grupo de Investigación en Ingeniería Aeroespacial, Universidad Pontificia Bolivariana, Medellín, Colombia*
[3]*Grupo de Investigación en Modelado, Electronica y Monitoreo (MEM), Faculty of Electronic Engineering, Universidad Santo Tomás, Bogotá, Colombia*
[4]*DTU Vindenergi, Risø Campus, Frederiksborgvej 399, Building 228, 4000 Roskilde, Denmark*
[5]*Department of Applied Mathematics III, Universitat Politècnica de Catalunya-BarcelonaTech, Comte d'Urgell 187, E-08036 Barcelona, Spain*
[6]*University of Siegen, Centre for Sensor Systems (ZESS), Siegen, Germany*
[7]*University of Siegen, Institute of Mechanics and Control Engineering-Mechatronics, Siegen, Germany*

SUMMARY

Damage assessment can be considered as the main task within the context of structural health monitoring (SHM) systems. This task is not only confined to the detection of damages in its basic algorithms but also in the generation of early warnings to prevent possible catastrophes in the daily use of the structures ensuring their proper functioning. Changes in environmental and operational conditions (EOC), in particularly temperature, affect the performance of SHM systems that constitutes a great limitation for their implementation in real world applications. This paper describes a health monitoring methodology combining the advantages of guided ultrasonic waves together with the compensation for temperature effects and the extraction of defect-sensitive features for the purpose of carrying out a nonlinear multivariate diagnosis of damage. Two well-known methods to compensate the temperature effects, namely optimal baseline selection and optimal signal stretch, are investigated within the proposed methodology where the performance is assessed using receiver operating characteristic curves. The methodology is experimentally tested in a pipeline. Results show that the methodology is a robust practical solution to compensate the temperature effects for the damage detection task. Copyright © 2015 John Wiley & Sons, Ltd.

Received 1 September 2014; Revised 12 January 2015; Accepted 13 January 2015

KEY WORDS: Damage Detection; Acousto-Ultrasonics; Signal Processing; Pattern Recognition; Wavelet Transform; Temperature Compensation

1. INTRODUCTION

The aim of an structural health monitoring (SHM) system is to reliably identify, at an early stage, the presence of damage that can lead to the failure of individual components or a system [1]. SHM systems are then a valuable tool for the assessment of the structural integrity in continuous operation for which a long-lasting suspension of their function for inspection is unwanted [2]. During the last decades, a huge amount of techniques for damage detection have been developed such as acoustic emission (AE), acousto-ultrasonics (AU), ultrasonic guided waves and standard ultrasonics [3–5].

The main difference between AE and AU lies in the fact that the first one is a passive sensing and the second one is an active sensing. That is, in AE, the occurrence of damages and their growth acts as

*Correspondence to: M.-A. Torres-Arredondo, MAN Diesel & Turbo SE, Engineering 4 Stroke-Test and Validation-Test Bed Management-Measurement (EETTM), D-86224, Augsburg, Germany.
†E-mail: m.a.torres.arredondo@gmail.com

the excitation signal. On the other hand, in AU, an external excitation signal is needed in order to analyze the wave interaction with damages. This last is one of the most important advantages of AU over AE. It is possible to excite the structure at any moment and study the wave correlations with damages. On the other hand, by means of AE, it is possible to detect evolving damages during in-service life of structures. Other notable work in the field of AE is given in [6–10].

The use of ultrasonic waves in SHM systems is a very attractive solution when large structural inspections are required. Nevertheless, additionally to the main problem related to the dispersive nature of waves (in case of thin-walled structures), a restricting factor for the practical use of SHM ultrasonic-based systems in field operation is the problem of distinguishing changes belonging to damage from the ones coming from changing environmental and operational conditions [11,12]. These sources of variability need to be identified and minimized in order to perform a reliable analysis and prognosis of the structural integrity.

A number of methods have been developed for compensating the effects of temperature. For example, Sohn used auto-associative neural networks for distinguishing extracted features related to damage from those caused by the environmental and vibration variations of the system [12]. Lu and Michaels computed differential features from diffuse ultrasonic signals and evaluated in terms of their efficacy under changing environmental conditions [13]. Mujica et al. explored the use of principal component analysis (PCA) and statistical distance measures to detect and distinguish damages in structures under varying EOC [14]. Other efficient temperature compensation strategies for guided wave structural health monitoring are discussed in detail in [13,15,16].

Farrar and Worden define that the SHM problem of damage detection can be essentially tackled as one of the statistical pattern recognition [2]. The idea is to extract features characterizing the normal condition, and then, these are used as a reference for comparison [17]. This approach was followed by Torres et al. in order to develop a nonlinear multivariate methodology for the purpose of damage detection and classification for AE and AU [18]. Within this methodology, new data were compared only with reference data from the same environmental conditions. However, this strategy is only appropriate when the normal condition does not vary with time. One possible solution to the problem is to collect the training data over a long time period in order to cover all the possible normal conditions [19]. Nevertheless, collecting data representative of the full population and all possible conditions for data-driven modelling is not an easy and realistic task for real world applications.

The purpose of this paper is to extend a previously developed methodology presented by the authors and to quantitatively analyze its performance by integrating different methods for temperature compensation. The work presented in this paper completes the studies presented in [20,21]. This paper is organized in six sections starting with this introduction. Section 2 includes a brief theoretical background about the different techniques used for feature extraction and nonlinear multivariate modelling within the extended methodology. Section 3 presents an experimental study of temperature variation on ultrasonic waves together with the techniques used for compensating the temperature effects. Section 4 explains in detail the damage assessment methodology. Finally, section 5 presents the experimental validation of the proposed methodology and section 6 the conclusions.

2. THEORETICAL BACKGROUND

2.1. Discrete wavelet transform

The discrete wavelet transform (DWT) is a powerful tool used in areas dealing with the analysis of transient signals and has been used by different authors in different applications normally focused on reduction in computational cost for signal processing tasks. This transform allows representing the variability of a given function at a specified time and scale by means of coefficients. According to Mallat, the DWT analysis is performed by means of a fast, pyramidal algorithm related to a two-channel sub-band coding scheme using a special class of filters called quadrature mirror filters [22]. Figure 1 shows a representation of the algorithm, where the signal $X(t)$ is analyzed at different frequency bands with different resolutions by means of approximation and detail coefficients. The detail coefficients are the low-scale, high-frequency components. The approximation coefficients represent

DOI: 10.1002/stc

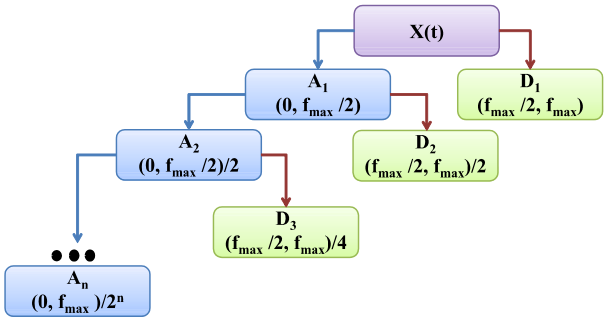

Figure 1. Multi-resolution analysis decomposition tree.

low-frequency components of the signal. The previously mentioned coefficients will be used as features in the process of damage detection (for further details, please refer to references [20,23]).

2.2. Hierarchical nonlinear principal component analysis

In many physical systems, there are only few 'forces' that drive the system. When this happens, it is possible to take advantage of the redundancies, simplifying the problem by replacing a group of variables with a new single 'virtual variable'.

PCA provides arguments on how to reduce complex dataset to a smaller dimension and also reveals simpler patterns or 'structures' that may be hidden under the data. The ultimate goal of the technique is to discern which data represent the most important dynamics of a particular system and which data, on the other hand, are redundant or just noise [24].

Over the years, several variations and improvements to PCA have been developed in order to deal with specific problems. Perhaps, one of the most common is nonlinear principal component analysis (NLPCA) that allows dealing with nonlinear problems in a better way than linear PCA. When nonlinear dependencies are present, a NLPCA model should be used instead of linear PCA. The NLPCA may be considered as a nonlinear generalization of the standard linear PCA. This generalization is achieved when the variables are projected onto surfaces or curves instead of planes or lines (like in PCA) [25].

As noticed by Scholz et al., NLPCA can be itself subdivided in two different variations: normal NLPCA and hierarchical NLPCA (h-NLPCA). The main difference between them is that h-NLPCA performs a dimensionality reduction by means of a hierarchical process. In this way, the data is decomposed in a PCA-related way [26]. Hierarchical NLPCA is based on multi-layered perceptron (MLP) architecture with an auto-associative topology. As with the traditional NLPCA, the network is performing an identity mapping where the output is forced to equal the input with high accuracy. In order to compress the data, there is a bottleneck layer in the middle with fewer units than the input and output layers that force the data to be projected into a lower dimensional representation (refer to Figure 2). Note that the nodes in the mapping and de-mapping layers must have nonlinear transfer functions; nonlinear transfer functions are not necessary in the bottleneck layer.

With the purpose of guaranteeing that the calculated nonlinear components have the same hierarchical order as the linear components in standard PCA, and in contrast to standard NLPCA, the reconstruction error is controlled by searching a k dimensional subspace of minimal mean square error (MSE) under the constraint that the $(k-1)$ dimensional subspace is also of minimal MSE [27]. This procedure is repeated for any $k-$ dimensional subspace where all subspaces must be of minimal MSE. It is expected that h-NLPCA will describe the data with greater accuracy and/or by fewer factors than PCA, provided that there are sufficient data to support the formulation of more complex mapping functions [27].

There are statistical tools, which used along with h-NLPCA, that allow the detection of anomalous behaviour in systems. The most common tool is the Q index (or squared prediction error (SPE)). The Q index indicates how well each sample fits the h-NLPCA model. It is a measure of the difference between a sample and its projection in the main components retained by the h-NLPCA model. It is based on analysis of residual data matrix $\widetilde{X}$ to represent the variability of the projection data in a sub residual space [25,28,29].

DOI: 10.1002/stc

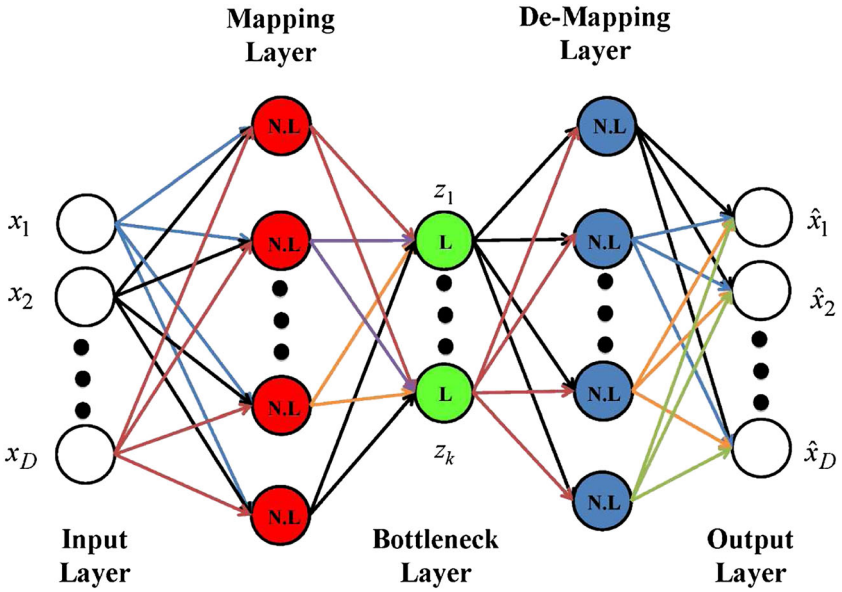

Figure 2. Network architecture for h-NLPCA.

The residuals of the h-NLPCA model can be assumed to follow a normal distribution because they represent insignificant variations attributable to uncorrelated variations and measurement uncertainty. These variations are not encapsulated in the nonlinear scores belonging to the h-NLPCA model [30].

For the h-NLPCA model, the residuals are given by

$$\widetilde{X} = \overline{X} - Pf\left(g\left(P^T\overline{X}\right)\right), \tag{1}$$

where P represents the principal components. Then, the Q index can be calculated as follows:

$$Q_i = \widetilde{x}_i\widetilde{x}_i^T = \overline{x}_i\left(I - P_rP_r{}^T\right)\overline{x}_i{}^T, \tag{2}$$

where $\overline{x}_i$ is the row vector of the original matrix, $\left(\overline{X}\right)$, $\widetilde{x}_i$ is the projection into the residual subspace and P_r represents the first r retained principal components $P_r = (p_1p_2 \ldots p_r)$

Because the Q index is a quadratic form of the errors and because these errors are well approximated by a multi-normal distribution, confidence limits also known as damage thresholds (based on Box's equation) can be defined as follows [31,32]:

$$UCL_Q = \delta^2 = \left(\frac{\upsilon}{2\varpi}\right)X^2_{2\varpi^2/\upsilon}(\alpha), \tag{3}$$

where $X^2_{2\varpi^2/\upsilon}(\alpha)$ is the upper (100 α)-th percentile of a chi-square distribution with $(2\varpi^2/\upsilon)$ degrees of freedom at significance level α, with ϖ and υ equal to the mean and the variance of the Q index sample, respectively.

2.3. ROC curves

Receiver operating characteristic (ROC) curves are a tool for diagnostic test evaluation, and they are well-known for describing the performance of diagnostic and detection systems in medical decision, signal processing and communications. These curves represent the trade-off between the false positive rate and the sensitivity for different cut-off points of a feature. The performance of the methods can be shown by the ROC curve that is made by sweeping a threshold value from high to low, that is, sweeping the false alarm rate from zero to one. The threshold is selected based on the statistics of signals

DOI: 10.1002/stc

recorded under the undamaged condition. Each point on the ROC curve represents a sensitivity/specificity pair corresponding to a particular decision threshold, and the area under the curve represents a measure that defined how well a parameter can distinguish between two groups. In the context of this work, these two groups represent the pristine and damaged condition of the structure. As curves bow more to the left, they indicate greater accuracy (a higher ratio of true positives to false positives). Accuracy is indexed more precisely by the amount of area under the curve, which increases as the curves bend [33].

ROC curves consisted in a unit square with the lower limit equal to zero and the upper limit equal to one on both axes (refer to Figure 3).

In hypothesis testing, a compromise between the false positive (commonly called error type I) and the false positive denoted by *FPi* and also commonly called error type II (defined as data corresponding to an undamaged case and classified as damaged) is needed because these two different types of errors cannot be reduced simultaneously. Therefore, the user needs to make decisions about which type of error is more critical in a particular application. For instance, in SHM applications, it might be more critical to minimize the false negative error denoted by *FNi* (defined as data corresponding to a damaged case and classified as undamaged), because an unchecked damage could lead to a catastrophic failure of a structure.

The classifier can be represented as one point in the ROC space (FP, TP) given by

$$(FP, TP) = \left(\frac{\sum FPi}{\sum Ni}, \frac{\sum TPi}{\sum Pi}\right), \tag{4}$$

where *TPi* (true positive) represents data corresponding to a damaged case and classified as damaged. The ROC curve is a graphical visualization of the true positive rate as a function of the false positive rate of a classifier, in this particular study, the *Q* index. Each *Q* index produces a single ROC point. The ROC curves can be obtained in several ways, for example, modifying the damage threshold. It produces a series of ROC points.

The area under the ROC curve (AUC) serves as comparison parameter, being a measurement of the accuracy of the classifier. The value of AUC is always between zero and one. If the AUC is close to one, the classifier presents a very good diagnostic test. The AUC represents the probability that the classifier will evaluate randomly chosen positive instance higher than a randomly chosen negative instance.

For calculating the ROC curves, the code published by Giuseppe Cardillo was used [34]. The cost-effective cut-off point was selected for calculate the performance. The cost-effective cut-off represents a point on the actual ROC curve whose distance from the upper left corner of the graph is minimal. It corresponds to the optimal cut-off value for the *Q* index.

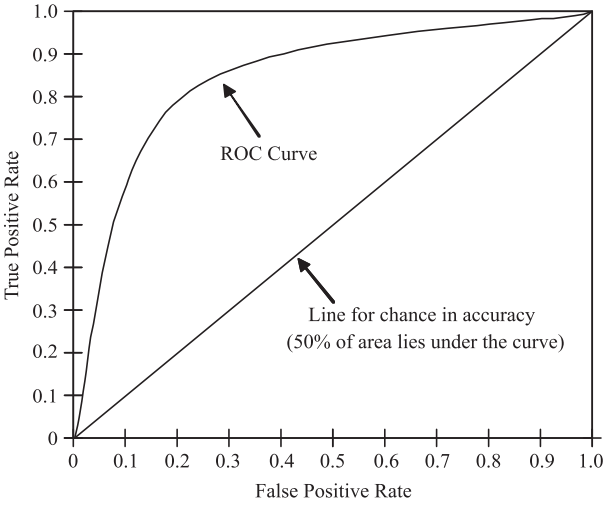

Figure 3. ROC curve.

DOI: 10.1002/stc

3. TEMPERATURE EFFECTS AND COMPENSATION TECHNIQUES

3.1. Effects of temperature on wave propagation characteristics

As it was discussed before, changing environmental conditions augment the complexity for the reliable monitoring of a structure. It is well known that temperature as well as damage can have similar effects on the dynamic behaviour of a structure. As a result, dynamic responses obtained for wave propagation-based methods can be affected by these effects and lead to false alarms or wrong damage locations. Therefore, it is very important to understand the impact of these changing conditions and take them into account. Well-known effects such as increase in time of flight and changes in sensor response magnitude with temperature [35] are analyzed and discussed in this section.

A plate made of six equal layers with a total thickness of 3 mm made of roving glass composite laminate from Bond Laminates GmbH is studied. The constitutive laminas were built with woven fibres. The experimental set-up is depicted in Figure 5(a) showing the structure with dimensions 200×250 mm. Temperature tests were conducted in a temperature-controlled oven. During the test runs, the temperature was raised stepwise from $T = 20 \pm 2°C$ up to $T = 60 \pm 2°C$. The temperature was measured by two PT100 sensors mounted on the plate opposite corners. Nine piezoelectric transducers PIC151 from PI Ceramics were attached to the surface of the structure. The structure was excited by a piezoelectric transducer located in the middle of the structure using pair of transducers operating in pitch-catch mode. The input signal to the actuators was generated using the arbitrary signal generation capability of a HandyScope HS3 (a combined signal generator and oscilloscope instrument manufactured by TiePie Engineering, Holland). The receiver sensors are connected to the input channels of an auxiliary HandyScope HS4. The processing engine for transmitting the waveform signal and acquiring the dynamic responses was written in Matlab® 7.9 using the DLLs provided by TiePie Engineering running under Windows operating system. The excitation voltage signal is a 12 V Hanning windowed tone burst with a carrier frequency of 50 kHz with 5 cycles. Sinusoidal signals with rectangular window or 'Hanning' windrow are usually used in AU applied to nondestructive testing and SHM in composite materials. These signals are called a 'tone burst'. An example of a 12 V Hanning windowed cosine train signal with 5 cycles at 50 KHz central frequency is presented in Figure 4. Transducer P5 was used as actuator.

The influence of the variation in temperature causes an evident change of the structural dynamics. The dynamic response signal for sensor number two, three and six decreased monotonically in peak-to-peak magnitude with increasing temperature, and it can be seen from Figure 5(b) to (d). According to experimental results depicted in Figures 5(b) to (d), the increase in the temperature causes a right time shift of the dynamic responses. Inversely, the decrease in the temperature causes a left shift. The reason of these time shifts is both thermal expansion and changes in wave velocities with temperature. The attenuation of the waves can be regarded to both wave dispersion as a result of frequency-

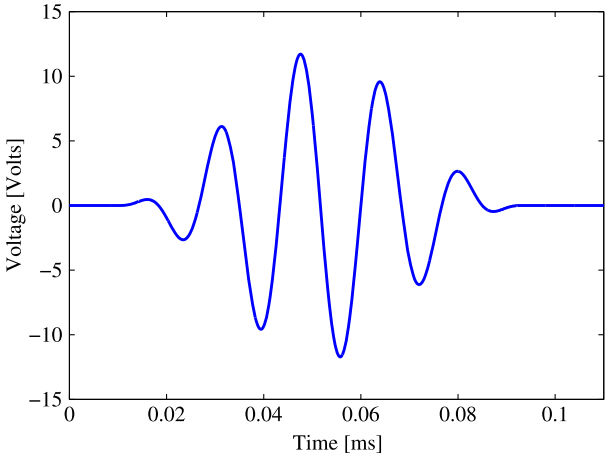

Figure 4. 12 V Hanning windowed cosine train signal with 5 cycles at 50 KHz central frequency.

DOI: 10.1002/stc

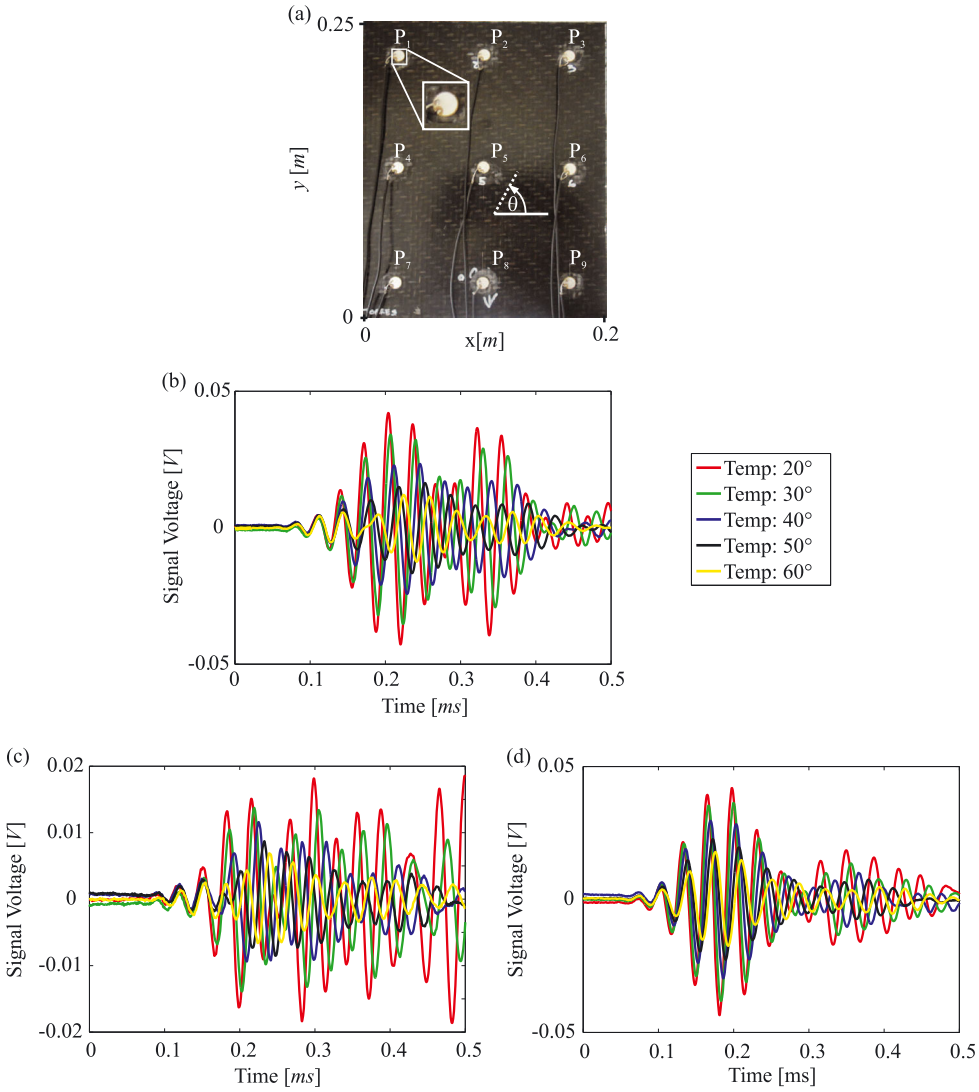

Figure 5. Influence of temperature on the propagated ultrasonic guided waves: (a) experimental set-up, (b) ultrasonic signals collected at transducer P2, (c) ultrasonic signals collected at transducer P3 and (d) ultrasonic signals collected at transducer P6.

dependent phase velocities and attenuation loss as a result of frequency/temperature-dependent material damping.

The second study carried out with this structure was performed in order to analyze the influence of the temperature cycles under which the structure was subjected at different excitation frequencies. Without loss of generality, the A_0 mode was selected in this study for the analysis of the influence of temperature gradient sign in the mode amplitude changes because this mode is easier to excite with the provided sensor arrangement.

The first effect that can be noticed from Figure 6(a) to (c) is the change of amplitudes for a given frequency and orientation of the sensor. This effect is explained because of the changing ratio of displacement and stress amplitudes with respect to the frequency and angular orientation for a particular mode along the plate thickness. As it can be inferred from all the results presented till now, the understanding of these wave propagation phenomena plays a critical role in the selection of the optimal inspection frequencies for the improvement of the sensitivity and for the optimization of sensor networks in terms of sensor placement and number of sensors. It can be observed as well that the temperature gradient has a strong effect on the trajectories of the peak-to-peak amplitudes with respect to the

DOI: 10.1002/stc

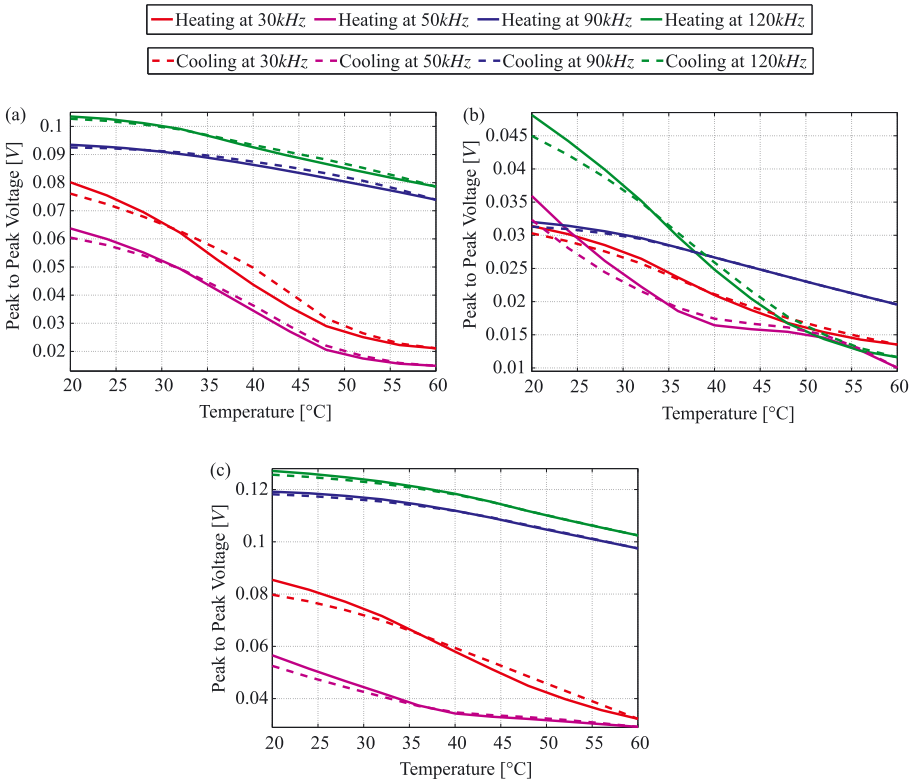

Figure 6. Temperature gradient effect on peak-to-peak amplitude of one of the contained modes (A_0).

heating or cooling cycles. It is good to bear in mind that the capacitance of piezoelectric materials is known to be temperature sensitive. As temperature increases, the capacitance value of the PZT normally increases and this effect modifies the response of the sensor. Even when not depicted for this plate, the dynamic response signals of all sensors decreased monotonically in peak-to-peak magnitude with increasing temperature for all the tested frequencies.

3.2. Temperature compensation techniques

As it was depicted before, temperature has a great influence on wave propagation. Approaches to overcome this problem are presented in [35,36] and are called optimal baseline selection (OBS) and optimal signal stretch (OSS). The OBS method is based upon a dataset of available baseline signals recorded at different temperatures. The idea behind this method is to select a single waveform $x(n)$ in the baseline dataset whose temperature is the closest to that of the monitored signal $y(n)$. According to Lu, the assumption is that the baseline waveform whose shape most closely matches that of the monitored signal is the one whose temperature is also the closest match [13]. In order to eliminate the effects of amplitude differences, Michaels and Michaels propose that the waveforms must be normalized in amplitude to obtain scaled waveforms [37]. The monitored signal (n) is normalized to unit energy:

$$y'(n) = \frac{y(n)}{\sqrt{\sum_{n=1}^{N} y(n)^2}}, \tag{5}$$

where N is the total number of samples of the discrete signal. The baseline waveform $x(n)$ is scaled to minimize the MSE between it, and the unity energy monitored signal $y'(n)$ as follows:

$$x'(n) = x(n)\frac{\sum_{i=1}^{N} x(i)y'(i)}{\sum_{i=1}^{N} x(i)^2}. \tag{6}$$

Finally, the normalized MSE E of the difference between the two scaled signals, which is used for

DOI: 10.1002/stc

the baseline selection, is calculated as [37]

$$E = \sum_{n=1}^{N} (y'(n) - x'(n))^2. \tag{7}$$

After finding the optimal baseline signal, the optimal signal stretch method is applied in order to further reduce the difference between the monitored signal and the optimal baseline. The method described here is exactly the same described by Croxford in [38]. This compensation is carried out in the frequency domain by stretching the frequency axis (stretch refers to both dilation and compression). The frequency step Δf of the monitored signal is increased or reduced until a minimum in the residual of the subtraction between it and the optimal baseline signal is achieved. Iterating this process yields to the optimal signal stretch between the two spectra, which corresponds to obtaining the minimum residual in the subtraction of the two signals in the time domain [39]. An example of using both techniques, that is, OBS + OSS, is depicted in Figure 7.

4. DAMAGE ASSESSMENT METHODOLOGY

To assess the structural integrity, a data-driven methodology is proposed. It consists of the analysis of data obtained from a structure instrumented with a piezoelectric distributed sensor network working in several actuation phases. At each actuation phase, a PZT is defined as actuator and the rest work as sensors collecting the information about the propagation of the excitation signal through the structure at different points. In this way, there are so many actuation phases as sensors in the system.

An AU approach is used to collect all the waveform energy that is available, that is, instead of selecting specific wave packets from the recorded signal, all the multiple reverberations are collected for their subsequent analysis. These dynamic responses collected from each actuation step, when the structure is known to be healthy, are pre-processed by the DWT in order to calculate the approximation coefficients. The two-channel sub-band coding scheme is applied to the recorded structural dynamic responses in order to produce a signal reconstruction to the level in which the signal could be properly reconstructed from the calculated coefficients with the minimum loss of information.

Determining the optimal basis function, that is, mother wavelet, for the signal decomposition is also a very important step in wavelet analysis because it guarantees an accurate decomposition of the original signal into the different frequency bands. The family of Daubechies wavelets ('db8') was chosen for this study. The optimum number of level decompositions was determined based on a minimum-entropy decomposition algorithm [40]. In this way, from the decomposition process, the approximation coefficients are obtained and stored into a matrix with dimensions ($E \times T$), where E represents the number of experiments and T the number of approximation coefficients for each defined baseline, that is, at different temperature ranges.

Denoting S as the number of piezoelectric transducers that are collecting the dynamical responses by each experiment, there are S matrices with the information from each sensor by each actuation step and

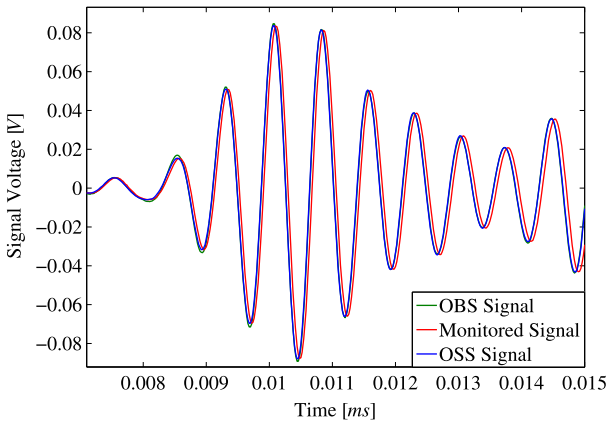

Figure 7. Process for OBS and OSS from a monitored signal.

DOI: 10.1002/stc

temperature range. Therefore, the whole set of the data collected in each actuation step and pre-processed by the DWT can be organized in a 3D matrix ($E \times T \times S$) or in a 2D matrix ($E \times TS$) where data from each sensor are located besides the other sensors for each temperature range by each actuation step as can it be seen in Figure 8. This step is very important within the proposed methodology because of the fact that different baselines at different temperature ranges are defined for each actuation step instead of generating a huge baseline including all the data. This provides the advantage of reducing variability in the models and increasing their sensitivity.

After this step, the matrices by each actuation step are pre-processed by means of group scaling method. This is carried out in order to remove the mean trajectories by sensor, and all sensors are made to have equal variance. Different methods can be used for this purpose; however, the authors found in a previous work that this method shows better results with this type of signals [41]. Using these pre-processed matrices, a statistical model using h-NLPCA is built for each actuation step at each temperature range using the approximation coefficients obtained from the undamaged structure data. Afterwards, the data from new collected structural responses in different states, that is, damaged or undamaged, are first temperature compensated using the OBS and OSS techniques. In the OBS technique, the best matching signal is searched along all of the stored baselines and then stretched with respect to the best match in the selected baseline.

Next, the DWT coefficients are extracted from the compensated responses, fused (as in the unfolding matrix previously explained) and projected into every model at the selected optimal baseline by each actuator in order to obtain the SPE indices. Subsequently, an outlier analysis is performed by each actuation step in order to determine the structural state. Figure 9 shows all the steps previously explained.

5. EXPERIMENTAL SET-UP AND RESULTS

In order to evaluate the practical performance of the proposed methodology, a pipeline is used as an experimental test bed. Figure 10 shows the pipeline that is instrumented with eight piezoelectric transducers PIC-151 from PI Ceramics at both ends of the structure. These are attached to the surface of the pipe with equidistant angular spacing on both sides at a distance of approximately 35 mm from the flanges. The piezoelectric transducers have a diameter of 10 mm and a thickness of 2.5 mm. The monitored pipe has a length of approximately 850 mm. It was made of stainless steel with an outer radius of 20 mm and 2.15 mm wall thickness.

In order to test the performance of the temperature compensation techniques inside the data-driven methodology, a first round of experiments were executed in order to collect data from the pristine condition. The temperature was varied in order to generate different datasets at several environmental conditions. For these experiments, baseline measurements were collected for a temperature span of

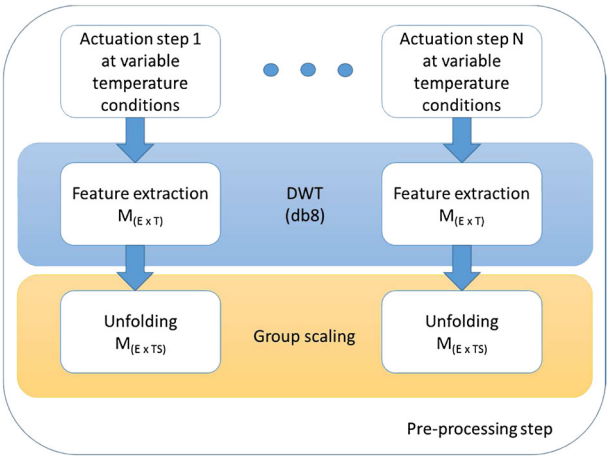

Figure 8. Pre-processing step.

DOI: 10.1002/stc

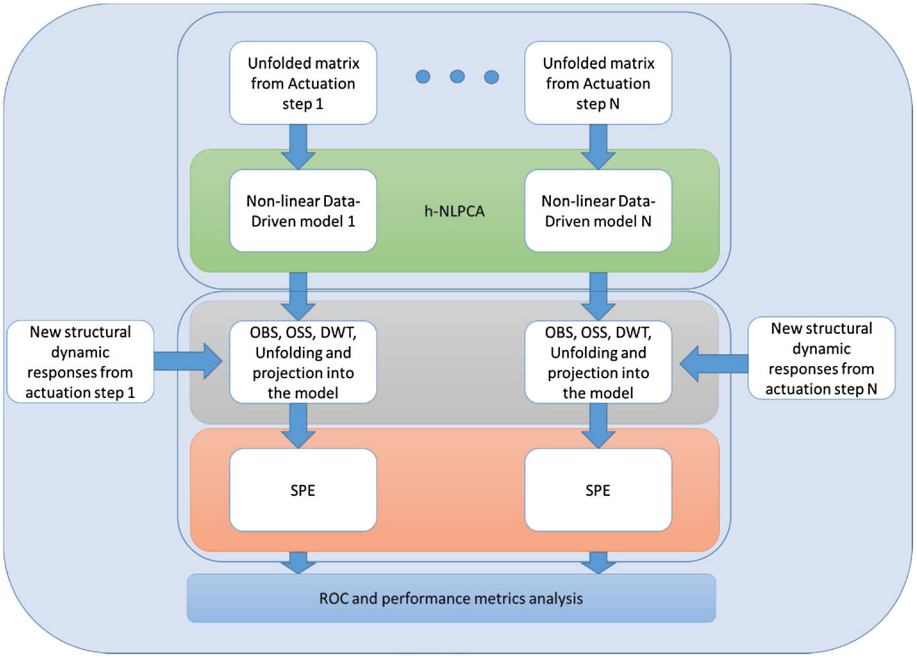

Figure 9. Methodology flow diagram.

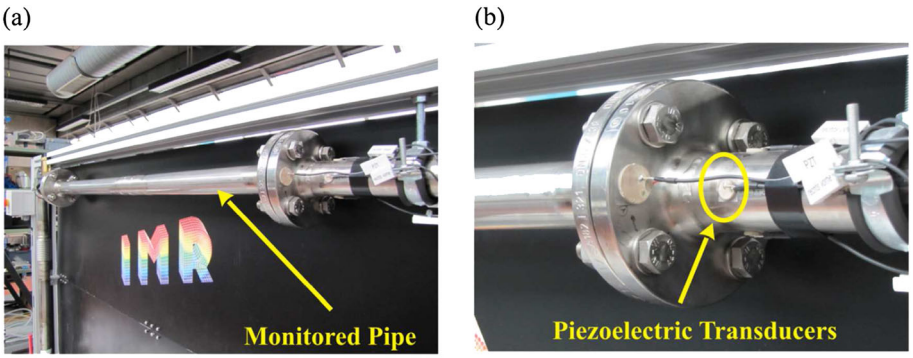

Figure 10. Experimental set-up.

approximately 23°C. Temperature varied from $T = 15$°C to $T = 38$°C. The temperature was measured by two PT100 sensors mounted on opposite corners of the pipe. The excitation voltage signal was a 12 V Hanning windowed cosine train signal with 5 cycles and carrier frequency of 136 kHz. The carrier frequency was chosen not only to maximize the propagation efficiency but also to specially excite the L (0,2) mode that provides an optimal wave energy distribution along the pipe's wall so that the detection capabilities of the system can be increased [42].

Afterwards, damage was introduced into the structure with an angular grinder, located close to the flange depicted in Figure 10(b) on the top of the pipe, in several steps and measurements that were recorded under similar environmental conditions to the ones mentioned before. The damage depth and its vertical extension were enlarged in four steps, starting with a cut of 0.3 mm depth. This cut was increased in depth in a second step until the wall was almost penetrated, followed by an increase in vertical direction. Finally, the pipe wall is penetrated, increasing the depth in the middle of the former notch.

Analyses of the baseline data for the purpose of the feature extraction step showed that a level 8 of decomposition was the optimal decomposition level for the discrete wavelet. After this step, a review of the variances retained in the components was performed in order to define the optimal number of components required for building the nonlinear models with the help of standard PCA. It was found that the first three components included around 90% of the total variance into the reduced model.

DOI: 10.1002/stc

For the experiments depicted here, 35 neurons were used for both hidden layers of the auto-associative neural networks for the different actuation steps. This value was found by searching a compromise between the dimensions in the mapping and de-mapping layers and the minimum reconstruction error generated by the network.

Once the models for each actuation step were generated by training the network, new data (under pristine and damaged conditions) were presented and processed according to the proposed methodology. An analysis of the ROC curves was then performed in order to depict the advantages of using the proposed methodology and to provide a statistical evaluation of its performance in comparison to traditional methods based solely on PCA projections.

Figure 11(a) and (b) show the ROC curves depicting the performance of the traditional procedure at each actuation step. As it could be seen, their performance is not so satisfactory. This is not surprising because the ability of the models is not robust to handle the experimental uncertainty because they either do not compensate the input data or do not include data that are representative of the conditions under which the classification is searched. This is further supported by the results depicted in Figure 12 (a) and (b) where the rate of false positives and negatives is relatively high. It can be seen from these results that the fused DWT features employed display a great sensitivity to temperature condition changes. Nevertheless, it is good to bear in mind that generating models able to properly generalize to the classification of new data, that is, models including data representative of the full population, could be a very expensive or even impossible process in real-life operating structures, and another strategy must be sought in order to tackle this problem.

In order to overcome this problem, an experimental application of OBS is considered and evaluated. In this analysis, only compensation by means of optimal baseline selection is carried out, that is, only one database of a group of several baseline databases at different temperature ranges for each actuation

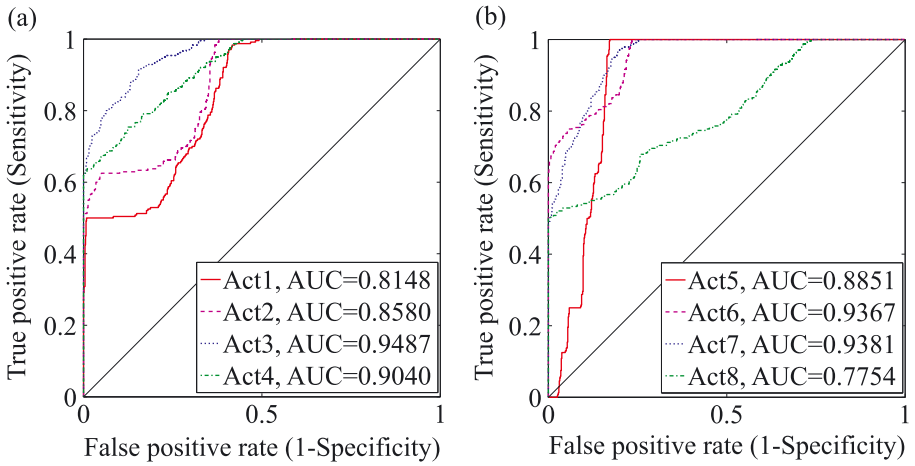

Figure 11. ROC curves for analysis without temperature compensation.

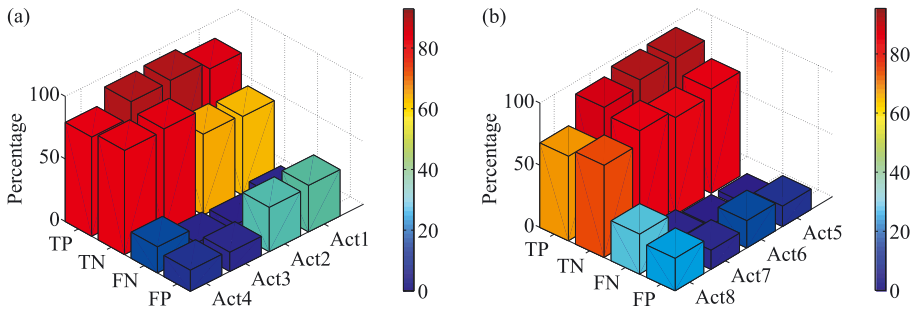

Figure 12. Prediction results without temperature compensation.

DOI: 10.1002/stc

step is selected. It is good to bear in mind that the OBS procedure only minimizes the temperature difference by selecting the database containing the baseline that which is more similar to the signal to be projected and does not modify the collected signals. According to Figures 13 and 14, there was a considerable improvement in the results after using the compensation method. These results validates that better discrimination may be possible if baseline signals at similar temperatures are used. It can be seen how the AUC is increased for every actuation step. and the rate of true positive and negatives is increased, that is, the probability of detecting damage and differentiating it from a simple temperature

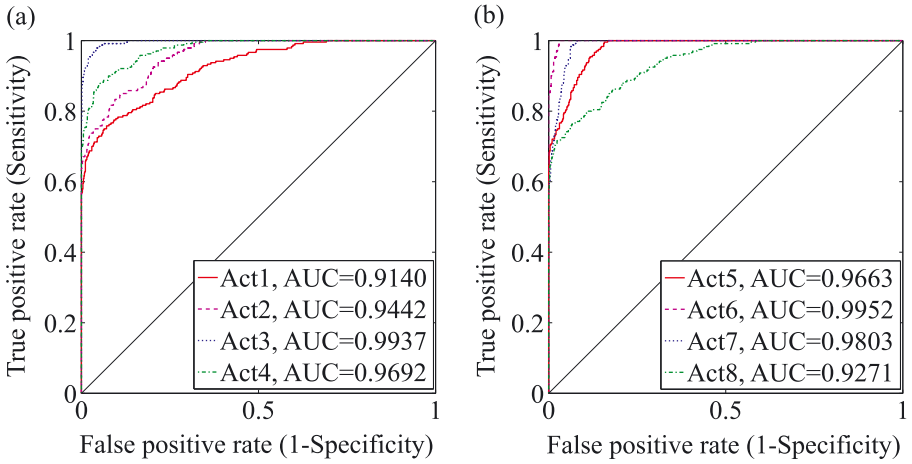

Figure 13. ROC curves for analysis only with OBS.

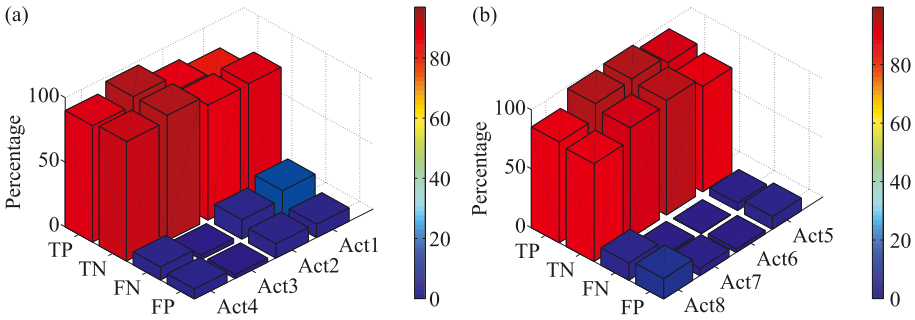

Figure 14. Prediction results only with OBS.

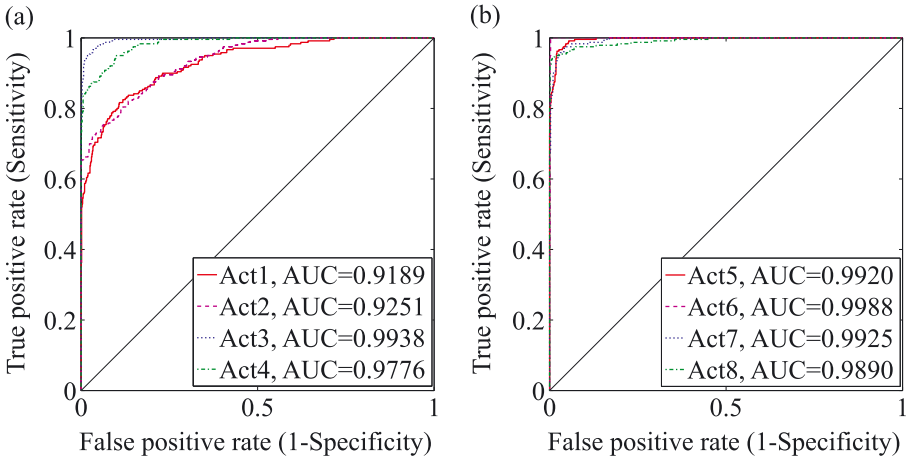

Figure 15. ROC curves for analysis with OBS + OSS.

DOI: 10.1002/stc

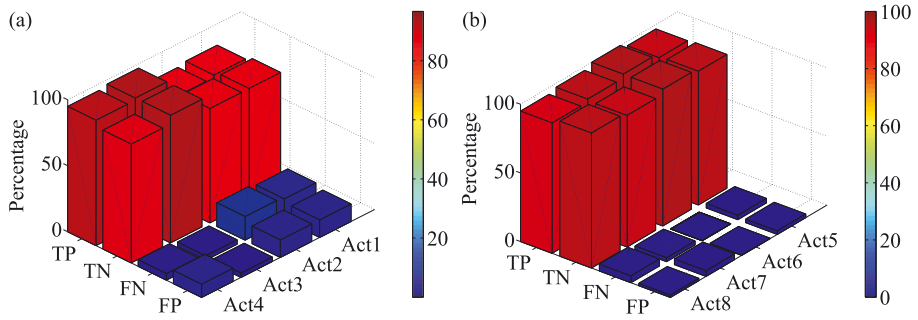

Figure 16. Prediction results with OBS + OSS.

change is also increased. Another way to see that all actuation steps have a better performance is given by the fact that the ROC curves in Figure 13(a) and (b) are closer to the upper left comer compared with the previously depicted curves.

Finally, the results obtained for the temperature effect compensation methodology using the OBS + OSS techniques through the experiments performed on the pipe are shown in Figures 15 and 16. It can be seen that the fusion of OBS and OSS for temperature compensation provides to a certain extent a better performance while using baseline models built with a reasonably small number of signals. This fact is of high importance because it validates the feasibility of the system for real-time monitoring in applications under temperature variations. Nevertheless, the biggest problem encountered during this study was the cost of recording enough baseline traces as a result of the necessity of acquiring data representative of the different environmental conditions under which the structure will operate. One observation is that all sensors located close to the damage provided a better performance for damage detection. This could be explained by the fact that the interactions of the incident waves with the damage and their response are less attenuated and consequently captured by the sensors located near to the damage in comparison to the sensors located far away. This observation also indicates the need to consider sensor placement for the design of the sensor network (maximum sensitivity with minimum sensor density). Of the three variants considered, the traditional multivariate approach is the least successful for detecting damage. The other two variants offered a higher likelihood for successful damage discrimination because they do take into consideration the time-varying nature of the signals as a result of temperature. As a future work, it would be interesting to analyze if there are obvious characteristics of the features that could distinguish damage from environmental changes. Similarly, it would be important to analyze the sensitivity of the system for the detection of damages with different severities.

6. CONCLUSIONS

The approach presented in this work is based on the analysis of ultrasonic signals from a piezoelectric active sensing system working on several actuation steps for the purpose of damage detection. In order to tackle the problem posed by temperature effects, a methodical temperature compensation strategy was proposed for structural health monitoring wave-based systems using AU.

Besides the temperature compensation, some relevant aspects related to AU must be taken into account when damage assessment is performed based on AU techniques. For instance, the selection of parameters such as the optimal number of cycles and excitation frequency together with an analysis of spreading of ultrasonic guided waves in space and time are important variables. The mode shapes of different guided wave modes need to be analyzed in order to depict the importance of the selection of the actuation signal for an optimized damage detection strategy. This is explained by the fact that it is possible that the modes that are excited in the structure could not be able to interact with damage. This is given because of the changing ratio of displacement and stress amplitudes along the wall thickness.

In the detection process, the compensation approach is based on the recording of a dataset of baseline signals covering the expected temperature range of operation of the structure followed by a feature

DOI: 10.1002/stc

extraction step together with multi-sensor data fusion and nonlinear modelling in which baseline selection and signal correction for each monitored signal is accomplished. This step allowed lessening the difficulty of analyzing directly the complex time traces by extracting relevant damage-related information and reducing the dimensionality of the problem. The proposed methodology was experimentally evaluated in a pipework with incremental real damage, and it was shown that the multivariate data-driven modelling methodology was a robust practical solution to temperature compensation and damage detection.

As it is well-known, influences such as temperature and changing operational conditions, which modify the structural dynamic responses, can be sufficient to disguise any changes correlated to damage to a level that it might not be detected. This fact makes, in the authors' opinion, automatic damage identification using data-driven methods still a very challenging task. Environmental and operational changes continue to represent a main concern for structural health monitoring systems, and robust techniques are still required to properly overcome this problem. These changes can be considered as one of the main disadvantages for implementing active guided wave-based techniques in real world applications. This is of special attention in baseline-based methods where the detection and characterization of damage are performed normally by means of metric indices by comparison of two dynamic response signatures.

Therefore, the influence of temperature must be compensated so that the damage assessment capabilities are not degraded. It is good to bear in mind that the effects of temperature on the transducer performance were not studied here. Nevertheless, it has been shown that these effects are significantly less than the effect of temperature on wave propagation within the structure. According to the authors' opinion, the development of an improved modelling technique incorporating the effects of variable temperature in wave propagation and sensor response as well as the analysis of sensor fault detection would be of great support for the design of a virtual SHM system.

ACKNOWLEDGEMENTS

The authors would like to express their gratitude to the Research School on Multi-Modal Sensor Systems for Environmental Exploration (MOSES) and the Centre for Sensor Systems (ZESS) for totally sponsoring the research presented herein. The authors would like to thank also Mr. Daniel Ocampo and Mr. Maximilian Scheid for their support during the experimental trials.

REFERENCES

1. Sohn H, Worden K, Farrar C. "Novelty detection under changing environmental conditions." in *In Proceedings of SPIE's 8th Annu. Int. Symp. on Smart Structures and Materials*, Newport Beach, 2001.
2. Farrar C, Worden K. An introduction to structural health monitoring. *Philosophical Transactions of the Royal Society A: Mathematical, Physical and Engineering Sciences* 2007; **365**(1851):303–315.
3. Mujica L, Rodellar J, Fernandez A, Güemes A. Q-statistic and T2-statistic PCA-based measures for damage assessment in structures. *Structural Health Monitoring* 2010; **10**(5):539–553.
4. Mustapha F, Manson G, Worden K, Pierce S. Damage location in an isotropic plate using a vector of novelty indices. *Mechanical Systems and Signal Processing* 2007; **21**(4):1885–1906.
5. Tibaduiza D-A, Torres-Arredondo M-A, Mujica L, Rodellar J, Fritzen C-P. A study of two unsupervised data driven statistical methodologies for detecting and classifying damages in structural health monitoring. *Mechanical Systems and Signal Processing* 2013; **41**(1-2):467–484.
6. Ohtsu M. The history and development of acoustic emission in concrete engineering. *Magazine of Concrete Research* 1996; **48**:321–330.
7. Carpinteri A, Lacidogna G, Pugno N. Structural damage diagnosis and life-time assessment by acoustic emission monitoring. *Engineering Fracture Mechanics* 2007; **74**:273–289.
8. Aggelis DG. Classification of cracking mode in concrete by acoustic emission parameters. *Mechanics Research Communications* 2011; **38**:153–157.
9. Behnia A, Chai HK, Shiotani T. Advanced structural health monitoring of concrete structures with the aid of acoustic emission. *Construction and Building Materials* 2014; **65**:282–302.
10. Carpinteri A, Grazzini A, Lacidogna G, Manuello A. Durability evaluation of reinforced masonry by fatigue tests and acoustic emission technique. *Structural Control and Health Monitoring* 2014; **21**:950–961.
11. Rytter A. "Vibration based inspection of civil engineering structures. PhD Thesis," Department of Building Technology and Structural Engineering, University of Aalborg, 1993.
12. Sohn H, Farrar C, Hunter N, Worden K. Structural health monitoring using statistical pattern recognition techniques. *Journal of Dynamic Systems, Measurement, and Control* 2001; **123**(1):706–711.
13. Lu Y, Michaels J. Discriminating damage from surface wetting via feature analysis for ultrasonic structural health monitoring systems. *Review of Progress in QNDE* 2008; **27**(1):1420–1427.

DOI: 10.1002/stc

14. Mujica L, Rodellar J, Worden K, Staszewski W. "Extended PCA visualization of system damage features under environmental and operational variations," in *Proc. SPIE 7286*, *Modeling*, *Signal Processing and Control for Smart Structures*, 2009.
15. Mujica L, Vehi J, Ruiz M, Verleysen M, Staszewski W, Worden K. Multivariate statistics process control for dimensionality reduction in structural assessment. *Mechanical Systems and Signal Processing* 2008; **22**(1):155–171.
16. Kraemer P, Buethe I, Fritzen C-P. "Damage detection under changing operational and environmental conditions using Self Organizing Maps," in *In Proceedings of SMART 11*, Saarbruecken, 2011.
17. Tibaduiza D. "Design and validation of a structural health monitoring system for aeronautical structures. PhD Thesis.," Departament de Matemàtica Aplicada III, Universitat Politècnica de Catalunya, 2013.
18. Torres-Arredondo M, Tibaduiza D-A, Mujica L, Rodellar J, Fritzen C-P. Data-driven multivariate algorithms for damage detection and identification: evaluation and comparison. *International Journal of Structural Health Monitoring* vol. DOI: 10.1177/1475921713498530, 2013.
19. Fritzen C-P, Mengelkamp G, Guemes A. "Elimination of temperature effects on damage detection within a smart structure concept," in *4th International Workshop on Structural Health Monitoring*,, Stanford, 2003.
20. Torres-Arredondo M, Fritzen C-P. "Ultrasonic guided wave dispersive characteristics in composite structures under variable temperature and operational conditions," in *6th European Workshop in Structural Health Monitoring*, Desden, 2012.
21. Moll J, Kraemer P, Fritzen C-P. "Compensation of environmental influences for damage detection using classification techniques," in *4th European Workshop on Structural Health Monitoring*, Krakow, 2008.
22. Mallat S. A theory for multiresolution signal decomposition: the wavelet representation. *IEEE Transactions on Pattern Analysis and Machine Intelligence* 1989; **11**(7):674–693.
23. Torres-Arredondo M. "Acoustic emission testing and acousto-ultrasonics for structural health monitoring. PhD Thesis.," Mechanical Engineering Department, University of Siegen, 2013.
24. Mujica L, Tibaduiza D, Rodellar J. "Data driven multiactuator piezoelectric system for structural damage localization," *Fifth world conference on structural control and monitoring*, 2010.
25. Jackson JE, Mudholkar GS. Control procedures for residuals associated with Principal Component Analysis. *Technometrics* 1979; **21**(3):341–349.
26. Scholz M, Fraunholz M, Selbig J. Nonliner principal component analysis: neuronal network models and applications. *Lecture Notes in Computational Science and Engineering* 2008; **58**:44–67.
27. Kramer M. Nonlinear principal component analysis using auto-associative neural networks. *AIChE Journal* 1991; **37**(2):233–243.
28. Villez K, Steppe K, De Pauw D. Use of unfold PCA for on-line plant stress monitoring and sensor failure detection. *Biosystems Engineering* 2009; **103**(1):23–34.
29. Burgos D, Mujica L, Güemes A, Rodellar J. "Active piezoelectric system using PCA," in *Fifth European Workshop on Structural Health Monitoring*, Sorrento, 2010.
30. Antory D, Kruger U, Irwin G, McCullough G. Fault diagnosis in internal combustion engines using non-linear multivariate statistics. *Journal of Systems and Control Engineering* 2005; **219**:243–258.
31. Nomikos P, MacGregor J. Multivariate SPC charts for monitoring batch processes. *Technometrics* 1995; **37**(1):41–59.
32. Wang X, Kruger U, Irwin G. Nonlinear PCA with the local approach for diesel engine fault detection and diagnosis. *IEEE Transactions on Control Systems Technology* 2008; **16**:122–130.
33. Vachtsevanos G, Lewis F, Roemer M, Hess A, Wu B. Intelligent Fault Diagnosis and Prognosis for Engineering Systems. John Wiley & Sons: New Jersey, 2006.
34. Cardillo G. "ROC Curve for Matlab," 2013. [Online]. (Available from: http://www.mathworks.com/matlabcentral/fileexchange/authors/22520.) [Accessed 1 09 2013].
35. Croxford A, Moll J, Wilcox P, Michaels J. Efficient temperature compensation strategies for guided wave structural health monitoring. *Ultrasonics* 2010; **50**(4-5):517–528.
36. Lu Y. "Analysis and modeling of diffuse ultrasonic signals for structural health monitoring. PhD Thesis.," School of Electrical and Computer Engineering, Georgia Institute of Technology, 2007.
37. Michaels J, Michaels T. Detection of structural damage from the local temporal coherence of diffuse ultrasonic signals. *IEEE Transactions on Ultrasonics Ferroelectrics and Frequency Control* 2005; **52**(10):1769–1782.
38. Croxford A, Wilcox P, Konstantinidis G, Drinkwater B. "Strategies for overcoming the effect of temperature on guided wave structural health monitoring.," in *SPIE 65321T*, 2007.
39. Cicero T. "Signal processing for guided wave structural health monitoring. PhD Thesis.," Department of Mechanical Engineering, Imperial College of Science, Technology and Medicine, 2009.
40. Coifman R, Wickerhauser M. Entropy-based algorithms for best basis selection. *IEEE Transactions on Information Theory* 1992; **38**(2):713–718.
41. Tibaduiza D, Mujica L, Rodellar J. Damage classification in structural health monitoring using self-organizing maps. *Structural Control and Health Monitoring* 2013; **20**(10):1303–1316.
42. Torres-Arredondo M, Buethe I, Tibaduiza D, Rodellar J, Fritzen C-P. Damage detection and classification in pipework using acousto-ultrasonics and non-linear data-driven modelling. *Journal of Civil Structural Health Monitoring* 2013; **4**:297–306.

DOI: 10.1002/stc